Journal of Ovonic Research Vol. 14, No. 4, July - August 2018, p. 261 - 267

SYNTHESIS, STRUCTURAL, OPTICAL AND MAGNETIC PROPERTIES OF $Zn_xCu_{0.5-x}Ni_{0.5}Fe_2O_4$ FERRITES BY CO-PRECIPITATION METHOD

G. MUSTAFA[a], M. U. ISLAM[a], H. ANWAR[b], M. ASIF[c], M. I. ARSHAD[d], N. SABAR[d], M. R. AHMAD[e], G. MURTAZA[f], M. A. BASHART[b], A. ALI[c], M. R. SALEEM[d], H. AKHTAR[*b]

[a]*Department of Physics, Bahauddin, Zakariya University Multan, 60800, Pakistan*
[b]*Department of Physics, University of Agriculture Faisalabad, 38040, Pakistan*
[c]*Department of Physics, COMSATS University Islamabad, Lahore Campus,Pakistan*
[d]*Department of Physics, G.C University, Faisalabad 38000, Pakistan*
[e]*Centre for Advanced Studies in Physics (CASP) G. C. University Lahore Pakistan*
[f]*Department of Physics,G.C.U. FSD. Layyah Campus,Layyah, 31200, Pakistan*

Zn-substituted Cu-Ni ferrite nanoparticles $Zn_xCu_{0.5-x}Ni_{0.5}Fe_2O_4$, (where $0 \leq x \leq 0.5$ with interval 0.1) have been synthesized using co-precipitation method which have been sintered at 900°C for 3 h. The X-ray diffraction (XRD) technique has been employed to confirm the single phase formation of spinel ferrite structure. The average particle size has been found in the range of 14-28 nm which has been estimated using Scherer's formula. The morphology of synthesized particle size has been confirmed using scanning electron microscopy (SEM). The size of particles has been found in close agreement with the XRD analysis. The optical band gap energy has been measured for x = 0.5 which have been found 2.3 eV. Moreover, the magnetic properties of sample x = 0.00 have also been observed. The saturation magnetization (M_s), remanance, Mr/Ms and coercive force have been observed. The obtained information of synthesized samples have super paramagnetic nature.

(Received April 11, 2018; Accepted July 4, 2018)

Keywords: Spinel ferrites, Co-precipitation Method, X-ray diffraction, M-H loop

1. Introduction

Spinel ferrites, with common formula of AB_2O_4 (where A is represent divalent and B is trivalent element) have wide technological applications such as electronic devices, computer devices, inter-body drug delivery (medication) rod antenna and humidity sensor [1] generally it is found that these metal ferrites have an inverse spinel cubic crystal structure in which half of the tetrahedral sites A-sites are occupied by Fe^{+3} ion. The octahedral sites B-sites will be held by the leftover Fe^{3+} with the transition metal ions (Ni^{2+}, Cu^{2+} or Zn^{+2}) [2]. In this study, we observed the effect of nonmagnetic ions (zinc and copper) with the replacement of ferromagnetic ions (nickel and iron) in a fixed proportion. The effect of these replacements on the structural, optical, and magnetic properties of synthesized ferrites has been observed which have been used as catalyst in some chemical processes as well as photo-catalyst [3]. Such ferrimagnetic materials have been studied extensively due to their low magnetic coercivity, high resistivity values and have small eddy current losses in high frequency operation [4]. It is well known fact that the properties of ferrite materials are strongly dependent on the material's composition. In addition to that the sintering conditions also put a strong influence for reducing the impurity levels [5]. The present synthesized materials give valuable information. At high temperature Zn^{2+} volatilization appeared in the formation of Fe^{3+} ions which caused the modification of the spinel structure after exchange of the cation distribution of the ions at the tetrahedral and octahedral sites [6]. Presently we synthesized the ferrites using co-precipitation technique [7-8] and main aims were to investigate

*Corresponding author: hassanakhtaruaf@gmail.com

the structural, optical and magnetic properties of $Zn_xCu_{0.5-x}Ni_{0.5}Fe_2O_4$ (x= 0.00, 0.1, 0.2, 0.3 and 0.5) spinel ferrites.

2. Experimental procedure

Polycrystalline spinel ferrites with composition $Zn_xCu_{0.5-x}Ni_{0.5}Fe_2O_4$ were prepared by co-precipitation method. The desired composition was obtained by taking stoichiometric amount of Ni $(NO_3)_2$ $6H_2O$, $Cu(NO_3)_2$ $6H_2O$, Zn $(NO_3)_2$ $3H_2O$ and $Fe(NO_3)_3$ $9H_2O$ were dissolved in deionized water. Ammonia solution was used to make the precipitate. The pH value of the solution becomes 10 and it was stirred for at least 1 h. The obtained precipitate ammonia solution then preheated water bath at 80 ^oC put beaker in water bath for 2 h during the digestion time the precipitate stalldown, the obtained precipitate washed with deionized water until it becomes free of impurities. The product was dried at 100 °C overnight to remove water contents. The dried powder was grinded with the help of mortar and pestle then calcinated at 900°C for 3 h. The X-ray diffraction (XRD) patterns were obtained at room temperature using powder samples in an Xpert Pro PANalytical diffractometer with Cu-Kα radiation (λ = 1.54056 Å) at 40 kV and 30 mA. Intensity data were collected by the step counting method (with a scanning speed 0.05°/s) in the 2θ range from 20-70°. The surface morphology and microstructure of the samples were studied by JSM-6490 JEOL scanning electron microscope (SEM). The elemental composition was determined by energy dispersive peak of the representative sample using energy dispersive X-ray spectroscopy (EDXS, Model JFC-1500 JEOL). The morphological studies were examined by using AFM (Digital instruments nanoscope-E, with Si_3N_4 100 nm cantilever, 0.58 N/m force constant) measurements in contact mode. The magnetic measurements were carried out at room temperature using vibrating sample magnetometer VSM, Lake Shore 735.

3. Result and discussion

3.1 Microstructural study

Fig. 1 shows XRD patterns for the spinel ferrite samples of Zn-doped Cu-Ni ferrites with composition $Zn_xCu_{0.5-x}Ni_{0.5}Fe_2O_4$ (x = 0, 0.1, 0.2, 0.3 and 0.4). All of the samples show the characteristic reflections of spinel cubic crystal structure of ferrite. No strong diffraction peaks of impurities were observed in the X-ray diffraction. The main spinel diffraction peaks were attributed to the (220), (311), (222), (400), (422), (511), and (440) planes [9]. The crystallite size, interplanar spacing distance, lattice constant, unit cell volume and X-ray density of all ferrite samples were calculated from the X-ray peak broadening of the (311) diffraction peak and have been listed in Table 1.

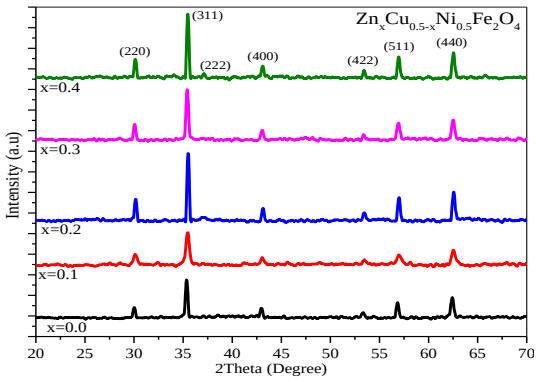

Fig. 1. XRD Patterns of $Zn_xCu_{0.5-x}Ni_{0.5}Fe_2O_4$ ferrites (x = 0, 0.1, 0.2, 0.3 and 0.4).

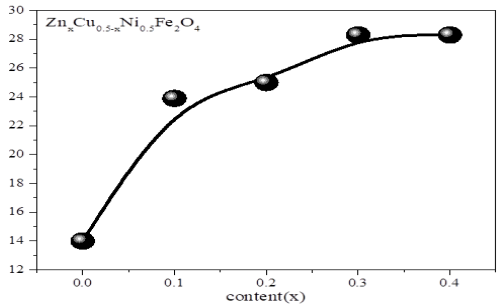

Fig. 3. Crystalline Size (nm) vs Content (x).

From Table 1, the average crystallite sizes was estimated from XRD data for all ferrite samples were approximately in the range 14-28 nm. Fig.2 showed a linear increasing trend in the crystallite size with the increase of the Zn^{+2}-concentration. The values of lattice parameters have been calculated by using the d-spacing values with their corresponding Miller indices (h k l) i.e. $\boldsymbol{a = \frac{\lambda}{2Sin\theta}\sqrt{(h^2 + k^2 + l^2)}}$ while the unit cell volume was determined in cubic spinel ferrites under these condition a = b = c while $\alpha = \beta = \gamma = 90^o$, $V_{cell} = a^3$ and was obtained values listed in the Table 1. The behavior of these parameters was shown in the Fig, 2. The cause of variation in the lattice parameters may be due to the difference of ionic radii. The Zn^{2+} (0.82 Å) ion has larger ionic radius than Ni^{2+} (0.78 Å) ion. The increase in Zn^{+2} substitution content consequently resulted in lattice expansion [10]. When Zn^{+} (0.82 Å) ions replaced with the Cu^{2+} (0.70 Å) ions, the lattice parameter of ferrite increased significantly from (8.3877 Å - 8.4222 Å) as listed in Table 1. The relationship lattice parameters and unit cell volume represent in the Fig.3. Moreover, The X-ray density D_x was calculated from the relation: $\rho_x = \frac{Z\,M}{N_A\,V}$ (where, V is primitive unit cell volume, Z denotes 8 molecules per unit cell of the spinel structure, M is the molecular weight of the sample and N_A is the Avogadro's number (6.02×10^{23} g/mol). The obtained values have been listed in the Table 1 that revealed the increasing trend with the increasing content (x) which have larger values as compared to the bulk density.

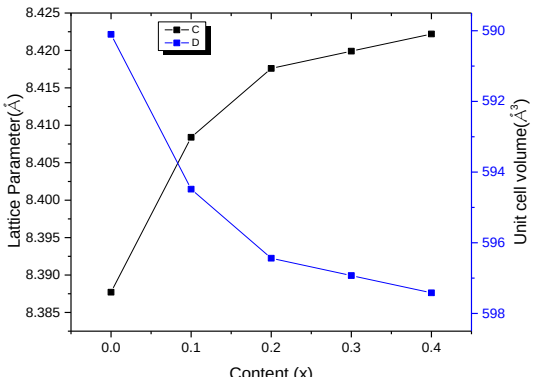

Fig. 3. Lattice Parameter and Unit Cell Volume versus Content (x).

Table 1. Crystallite size (nm), Lattice constant (a), volume of the unit cell and X-ray density (d_x) Zn^{+2}-substitution of $Zn_xCu_{0.5-x}Ni_{0.5}Fe_2O_4$ ferrites.

Composition	Crystallite Size (nm)	Lattice Constant (Å)	Volume of the unit cell (Å^3)	d_x (g/cm^3)
$Cu_{0.5}Ni_{0.5}Fe_2O_4$	14	8.3877	590.12	5.33
$Zn_{0.1}Cu_{0.4}Ni_{0.5}Fe_2O_4$	23.9	8.4084	594.59	5.34
$Zn_{0.2}Cu_{0.3}Ni_{0.5}Fe_2O_4$	25	8.4176	596.57	5.36
$Zn_{0.3}Cu_{0.2}Ni_{0.5}Fe_2O_4$	28.3	8.4199	596.92	5.43
$Zn_{0.4}Cu_{0.1}Ni_{0.5}Fe_2O_4$	28.3	8.4222	597.41	5.47

3.2 Morphological and texture and elemental analysis

The SEM images of $Zn_xCu_{0.5-x}Ni_{0.5}Fe_2O_4$ (x = 0, 0.1, 0.2, 0.3 and 0.4) ferrites samples were shown in Fig. 4. The SEM image exhibited the shape of nanoparticles which were in spherical shape with different sizes over a particular scanned area [11]. The distribution of the grain was found uniform. It has been clearly seen from the images of the grain that their size varied with the increase of the Zn content (x), which has been disbursement of cation positions in lattice [12]. Moreover from Fig. 5, the texture of the prepared sample was also observed with the atomic force microscopy (AFM). These images showed the complimentary information about the surface microstructure, grain size distribution and roughness of the surface of the prepared sample of x= 0.2.

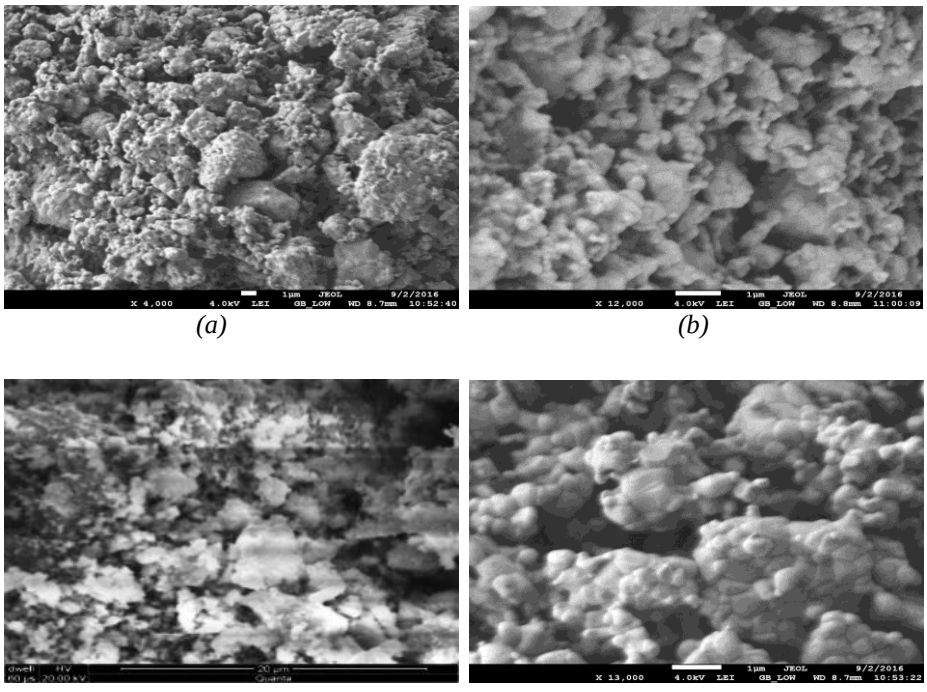

(a) *(b)*

(c) *(d)*

Fig. 4. Morphological analysis for $Zn_xCu_{0.5-x}Ni_{0.5}Fe_2O_4$ (a) x= 0.00, (b) x= 0.1, (c) x= 0.2, and (d) x= 0.3

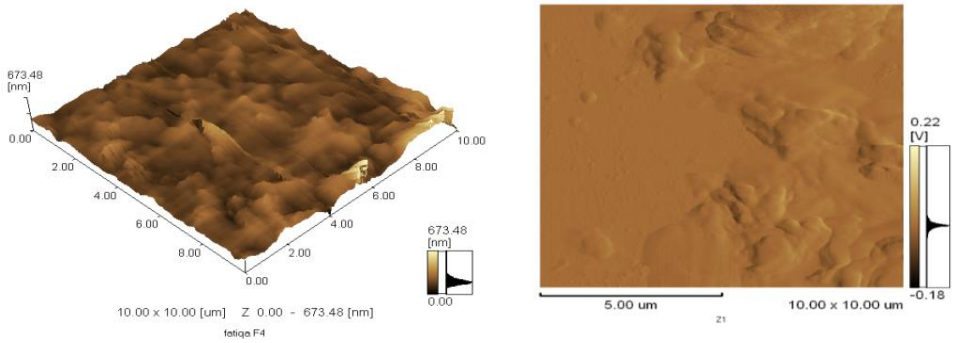

(a) *(b)*

Fig. 5. AFM images of $Cu_{0.5}Ni_{0.5}Fe_2O_4$ spinel ferrite x = 0.00 (a) 3D and (b) 2D

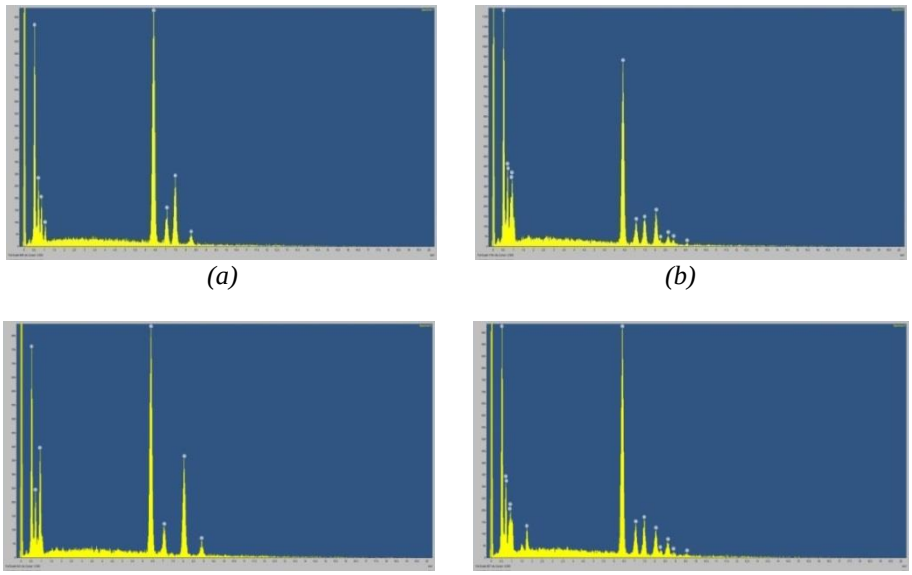

(a) *(b)*

(c) *(d)*

Fig. 6. EDX Spectrum for $Zn_xCu_{0.5-x}Ni_{0.5}Fe_2O_4$ (a) x= 0.00, (b) x= 0.1, (c) x= 0.2, and (d) x= 0.3

The observed appearance of the grain by AFM was also consistent with the results of SEM analysis [13]. Fig. 6 showed the energy dispersive spectrum of the ferrites sample for different concentrations. The observed atomic percentages (%) of Ni, Zn, Cu, Fe, and O elements in the prepared nanoparticle samples have been tabulated in the Table 2. The EDX analysis confirmed that there was no impurity in the prepared samples [14]. The observed composition and atomic % of each element has been listed in the Table 2.

Table 2. The Elemental Composition of $Zn_xCu_{0.5-x}Ni_{0.5}Fe_2O_4$.

Elements	**X =0.00**	**X= 0.1**	**X = 0.2**	**X = 0.3**	**X = 0.4**
O Atomic (%)	50.65	46.21	51.47	47.83	39.72
Fe Atomic (%)	28	31.7	27.43	29.8	40.6
Ni Atomic (%)	11.47	10.12	8.64	9.77	8.56
Zn Atomic (%)	-----	2.25	4.51	7.26	8.59
Cu Atomic (%)	9.88	9.72	7.95	5.34	2.53

3.3 Optical properties

Fig. 7 illustrates the UV/Vis spectra of sample at x = 0.5. The absorbance of the Zn prominently was observed in the region wavelength 227-382 nm while another intense peak at 923 nm and representing the presence of oxygen-containing groups linked with a cubic structure [15]. Moreover, the optical band gap and the absorption coefficient (α) of the synthesized ferrites was calculated by Eq. 1.

$$\alpha h\nu = \mathrm{A}(h\nu - E_g)^n \tag{1}$$

where 'α' is the linear absorption coefficient of the material, hν is the photon energy 'A' is a constant of proportionality, E_{gap} is the optical band gap energy and 'n' is a constant related with different kinds of electronic transitions (n = 1/2 and 2 for a direct and indirect allowed respectively) [16]. In this Fig. 7 shows the band gap energy of the sample measured 2.3 eV at n = 0.5.

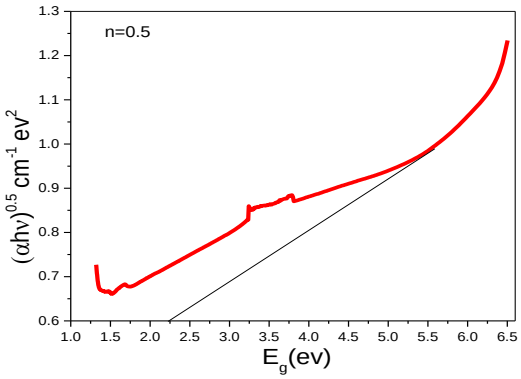

Fig. 7. The optical band gap and the absorption coefficient of $Zn_{0.5}Ni_{0.5}Fe_2O_4$.

3.4 Magnetic measurements

Fig. 8 shows the magnetic behavior of $Cu_{0.5}Ni_{0.5}Fe_2O_4$ spinel ferrites powder which have been annealed at 900 ^oC. The values of both saturation magnetization and remanance were found 50 emu/g and 12.7 emu/g respectively at x = 0.00. It shows that the Zn^{2+}, Cu^{2+} ions occupy A-site and Ni^{2+} ions preferably enters (B-site) octahedral. The number of Fe^{3+} at B-sites decreases with the replacement of Ni^{2+} ions due to which the magnetization of B-sublattice strengthen. The remanance ratio (Mr/Ms) of the sample is observed 0.25 (well below of typical value ~1) [17]. It is found that the soft spinel ferrites have 154 Oe-coercive force of the sample at x = 0.00.

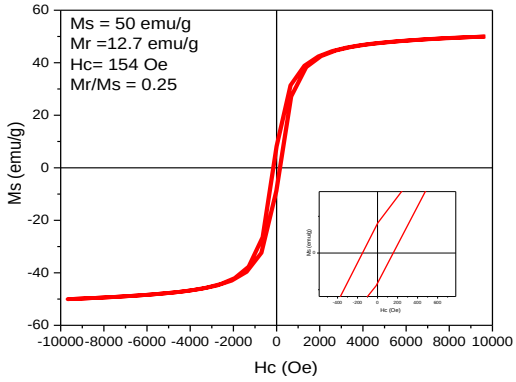

Fig. 8. M-H loops for $Cu_{0.5}Ni_{0.5}Fe_2O_4$ ferrite powders.

4. Conclusions

A series of $Zn_xCu_{0.5-x}Ni_{0.5}Fe_2O_4$ (x = 0, 0.1, 0.2, 0.3 and 0.4) spinel ferrites has been successfully synthesized by co-precipitation methods and has also been analyzed via XRD. The lattice constant was found in the range 8.3877 Å - 8.4222 Å and the average crystallite size in the range of 14 -28 nm was calculated using Scherrer's formula.

From Scanning electron microscopy analysis, it had observed agglomeration of the particles which was found due to high temperature. The optical band gap energy was observed at x = 0.5 was 2.3 eV which is due to the formation of oxygen vacancies and the induction of lattice distortions. SEM analysis confirmed the morphology of the synthesized material and growth of grain size. The magnetic properties of the synthesized sample suggested that it had super paramagnetic in nature.

Acknowledgements

The author is thankful for providing characterization support to carry out this work under Govt. College University Faisalabad-RSP-Project # 159-PHY-5

References

[1] Bai Jianmin, Jian-Ping Wang. Applied Phy.Letters **87**(15), 152502 (2005).
[2] Kavas, Hüseyin, Abdülhadi Baykal, Muhammet S. Toprak, Yüksel Köseoğlu, Murat Sertkol, Bekir Aktaş, J. Alloy & Comp. **479**(1-2), 49 (2009).
[3] R. Ch. Che, L. M. Peng, Xiao Feng Duan, Qing Chen, X. L. Liang. Advanced Materials **16**(5), 401 (2004).
[4] Tsay, C. Y., K. S. Liu, T. F. Lin, I. N. Lin. J. Magn.and Magn. Mate. **209**(1-3), 189 (2000).
[5] Shi-Yong Zhao, Ru Qiao, Xiao Li Zhang, Young Soo Kang The Journal of Physical Chemistry C **111**(22), 7875 (2007).
[6] M. Sertkol, Y. Köseoğlu, A. Baykal, H. Kavas, A. Bozkurt, Muhammet S. Toprak. J. Alloy. Comp **486**(1-2), 325 (2009).
[7] M. Atif, M. Nadeem, R. Grössinger, R. Sato Turtelli, J. Alloy.Comp **509**(18), 5720 (2011).
[8] Yen-Pei Fu, Shao-Hua Hu, Ceramics Inte. **36**(4), 1311 (2010).
[9] T. T. Ahmed, I. Z. Rahman, M. A. Rahman, Journal of Mate. Proc. Techn. **153**, 797 (2004).
[10] M. J. Iqbal, M. R. Siddiquah, J. Magn. and Magn. Mate **320**(6), 845 (2008).
[11] R. G. Kharake, R. S. Devan, B. K. Chougalu, J. of Alloys and Comp. **463**, 67 (2008).
[12] Y. Dasan et al., PloS one **12**(1), 0170075 (2017).
[13] C. Stergiou, G. Litsardakis. Conference Proceedings. 2014. AIP.
[14] Y. Wang et al. J. Magn.and Magn. Mate,. **398**, 90 (2016).
[15] G. Mustafa et al., J. Magn.and Magn. Mate. **378**, 409 (2015).
[16] G. Mustafa et al., J. Magn. and Magn. Mate. **387**,147 (2015).
[17] N. Amin et al., Digest Journal of Nanomaterials and Biostructures. **11**(2), 579 (2016).